Heat of Reaction in Individual Metabolic Pathways of Yeast Determined by Mechanistic Modeling in an Insulated Bioreactor

Yusmel González-Hernández, Emilie Michiels, Patrick Perré

Graphical Abstract

Heat of Reaction in Individual Metabolic Pathways of Yeast Determined by Mechanistic Modeling in an Insulated Bioreactor

Yusmel González-Hernández, Emilie Michiels, Patrick Perré

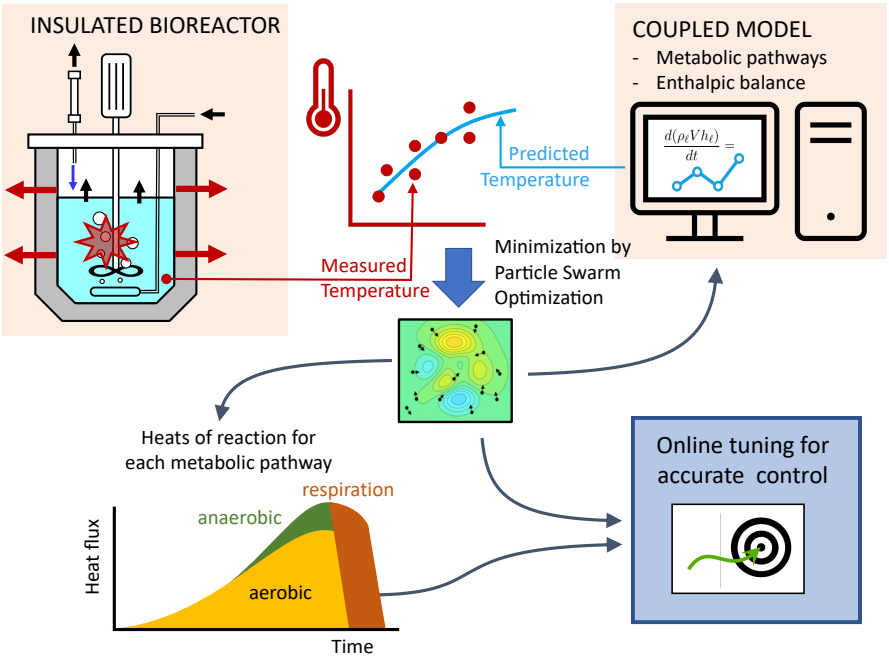

Heat of Reaction in Individual Metabolic Pathways of Yeast Determined by Mechanistic Modeling in an Insulated Bioreactor

Yusmel González-Hernández[1], Emilie Michiels[1†], Patrick Perré[1*†]

[1]Université Paris-Saclay, CentraleSupélec, Laboratoire de Génie des Procédés et Matériaux, Centre Européen de Biotechnologie et de Bioéconomie (CEBB), 3 rue des Rouges Terres, Pomacle, 51110, France.

*Corresponding author(s). E-mail(s): patrick.perre@centralesupelec.fr;
Contributing authors: yusmel.gonzalez-hernandez@centralesupelec.fr;
emilie.michiels@centralesupelec.fr;
†These authors contributed equally to this work.

Abstract

Background

The yeast *Saccharomyces cerevisiae*, commonly used in industry, exhibits complex metabolism due to the Crabtree effect, fermenting alcohol even under aerobic conditions when glucose exceeds 0.10-0.15 g/L. The heat released by the biological activity is a signal very easy to collect, given the minimal instrumentation requirements. However, this heat depends on the activated metabolic pathways and provides only an indirect indicator, that cannot be used in a simple way. This study demonstrated the potential of a mechanistic model to control the process by measuring the heat released by the biological activity.

Results

The complexity arising from coexisting metabolic pathways was addressed by a comprehensive model of *Saccharomyces cerevisiae* together with the heat of reaction included in a rigorous enthalpy balance of the bioreactor. Batch cultures were performed in an insulated bioreactor to trigger a temperature signal. The heat of individual metabolic pathways was determined by inverse analysis of these tests using Particle Swarm Optimization (PSO): -101.28 ±0.02kJ/mol for anaerobic fermentation, -231.27±0.06kJ/mol for aerobic fermentation, and -662.94 ± 0.54kJ/mol for ethanol respiration. Finally, the model was successfully applied and validated for online training under different operating conditions.

Conclusions

The model demonstrates remarkable accuracy, with a mean relative error under

0.38% in temperature predictions for both anaerobic and aerobic conditions. The viscous dissipation is a key parameter specific to the bioreactor and the growth conditions. However, we demonstrated that this parameter could be fitted accurately from the early stages of the experiment for further prediction of the remaining part. This model introduces temperature, or the thermal power required to maintain temperature, as a measurable parameter for online feedback model training to provide increasingly precise feed-forward control.

Keywords: yeast, fermentation, heat of reaction, metabolic pathway, modeling, calibration

Abbreviations

A	Heat exchanging area (m^2)
C_p	Specific heat (J/kg/K)
$EtOH$	Ethanol concentration (g/L)
F	Volumetric flow (m^3/s)
Glc	Glucose (kg/m^3 = g/L)
Glc_c	Mean value of the glucose transition range (kg/m^3 = g/L)
Gly	Glycerol concentration (kg/m^3 = g/L)
h	Specific enthalpy (J/kg)
h_{dry}	Specific enthalpy of dry air (J/kg of dry gas)
H	Enthalpy of reaction (J/mol)
RH	Relative humidity
k_La	Overall oxygen transfer rate (s^{-1})
L	Latent heat coefficient (J/kg)
M	Molar mass (kg/mol)
O_2	Oxygen concentration (kg/m^3 = g/L)
O_2^*	Oxygen saturation concentration (kg/m^3 = g/L)
P	Pressure (Pa)
q	Mass flow (kg/s)
q_h	Heat power (W)
Q	Biological heat released (J)
R	Volumetric growth rate ($kg/m^3/s$)
S	Substrate concentration (kg/m^3 = g/L)
SD	Standard deviation
T	Temperature (℃)
X	Yeast concentration (kg/m^3)
Y	Biological yield coefficient (kg/kg)/Absolute moisture content (kg of vapor/kg of dry g
V	Volume (m^3)
Greek symbols	
α	Sharpness of transition function
Δ	Variation
μ	Specific growth rate (s^{-1})
λ_f	Transition function
ρ	Density (kg/m^3)
ω	Water mass content in gas (kg of water/kg of gas)
Subscripts	
1	Anaerobic fermentation (ANF)
2	Aerobic fermentation (AF)
3	Glucose respiration (GR)
4	Ethanol respiration (ER)
a	Air
atm	Atmospheric
Ax	Anaerobic operating condition mode
$cold$	Relative to the cold finger
$cond$	Condensation
dry	Dry gas (air or nitrogen)
e	Experimental
ext	Associated to laboratory room
g	Gas
in	Inlet
ℓ	Liquid water
$loss$	Losses to the environment
m	Model
out	Outlet
Ox	Aerobic operating condition mode
$stor$	Stored
sv	Saturated vapor
$visc$	Viscous dissipation
w	Water
$yeast$	Associated to yeast activity

1 Background

The yeast *Saccharomyces cerevisiae* is one of the most commonly used yeasts in the industry (Parapouli et al, 2020; Guo et al, 2023; Nya and Etukudo, 2023). However, this yeast exhibits a somewhat complex metabolism due to its positive response to the Crabtree effect. This yeast carries out alcoholic fermentation under anaerobic conditions but can do so under aerobic conditions when the glucose concentration exceeds 0.10-0.15 g/L. When the glucose concentration is below these values, it solely performs respiration (Verduyn et al, 1984). Hence, during aerobic conditions, the metabolism of this yeast will be primarily governed by glucose concentration, which can be regulated by the feed input. However, this would require continuous control of the glucose concentration in the medium to program the feeding accordingly. In this sense, several methods have been developed to control yeast metabolism using variables that can be directly measured during cultivation: dissolved oxygen, optical density, Raman spectroscopy, pH, pressure, exit gas composition, and metabolic heat flow (Lee et al, 1999; Claes and Van Impe, 2000; Türker, 2004; Ingledew and Lin, 2011; Biener et al, 2012; Yang et al, 2024). The latter method is notably simple due to its minimal instrumentation requirements, primarily grounded on the consistent heat production accompanying microbial metabolism. An additional benefit of utilizing biological heat as a metabolism indicator is its capacity to offer insights into the stoichiometry and kinetics linked to the process, allowing immediate observation of changes upon the activation of the metabolic pathways, according to the operating conditions (Auberson and Von Stockar, 1992; Duboc et al, 1998; Von Stockar et al, 2006; Maskow et al, 2011; Biener et al, 2012).

This method has already been used as a reliable biomass monitoring tool and as a key part of a robust control strategy for aerobic fed-batch cultures, where the dilution rates were controlled by estimating the specific yeast growth rates as a function of the metabolism heat release. The capacity to maintain yeast growth by glucose respiration using heat measurements as indirect means to determine and regulate the system was proved in Biener et al (2012). Similarly, in less complex strains such as *Escherichia coli*, *Candida utilis*, *Kluyveromyces marxianus*, and *Pichia pastoris* this technique has been successfully tested (Biener et al, 2010; Schuler et al, 2012). Nevertheless, applying this technique to *Saccharomyces cerevisiae* for ethanol production, under aerobic conditions becomes more complex due to the coexistence of metabolic pathways based on the same substrate (e.g., glucose fermentation and glucose respiration, ethanol production and ethanol respiration) (Sonnleitner and Käppeli, 1986; González-Hernández et al, 2022).

Undoubtedly, a viable solution to tackle this challenge lies in mechanistic modeling. This approach allows the prediction of crucial biological and physical variables during fermentation accounting for substrate limitations and the inhibition effect of ethanol. Owing to the application of these predictive tools, real-time physical parameters such as temperature can be used to determine the specific contributions of each metabolic pathway by inverse analysis. Accordingly, this study proposes a comprehensive model considering the metabolic pathways of yeast *Saccharomyces cerevisiae*, their associated biological heat and the physical transfers within the bioreactor to predict the temperature. To archive this goal, the model combines a mechanistic model

of the metabolic pathways with an enthalpy model involving the heats of reaction. Several cultures with contrasted conditions were performed in an insulated bioreactor: this allows the biological heat released during the culture to trigger a temperature signal. Through inverse analysis, parameters poorly documented in the literature, such as reaction enthalpies associated with each metabolic pathway, as well as the physical parameters of the bioreactor, are estimated.

2 Materials and methods

2.1 Experimental setup

A 5-liter Sartorius Biostat B Plus bioreactor (Fig. 1) was used in batch mode for cultivating the *Saccharomyces cerevisiae* strain IOC Fizz+ (active dry yeast), which is alcohol-resistant up to 14% vol. and possesses the killer factor (K2)(González-Hernández et al, 2022). The fermentation utilized a YPD culture medium with varying glucose concentrations (15-30 g/L), 20 g/L of peptone, and 20 g/L of yeast extract. The bioreactor was stirred at 295 rpm, with continuous injection of 500 cm^3/min of air for the aerobic process, while the same flow of nitrogen was used for strict anaerobic conditions. Foaming was controlled by adding silicone antifoam (Chem-Lab). A cooling finger was attached to the gas outlet to reduce ethanol and water losses. In the bioreactor, pH and dissolved oxygen levels were measured using internal Hamilton electrodes, while temperature was monitored using an internal Sartorius Pt-100 probe. The inlet and outlet gas humidity and temperature were measured using SHT85 Sensirion sensors (letters S in Fig. 1). The room temperature was also recorded during all experiments using an SHT85 sensor placed near the bioreactor. For this study, the Biostat was not used to regulate the bioreactor temperature. Instead, the bioreactor was insulated to generate the temperature signal used throughout this work.

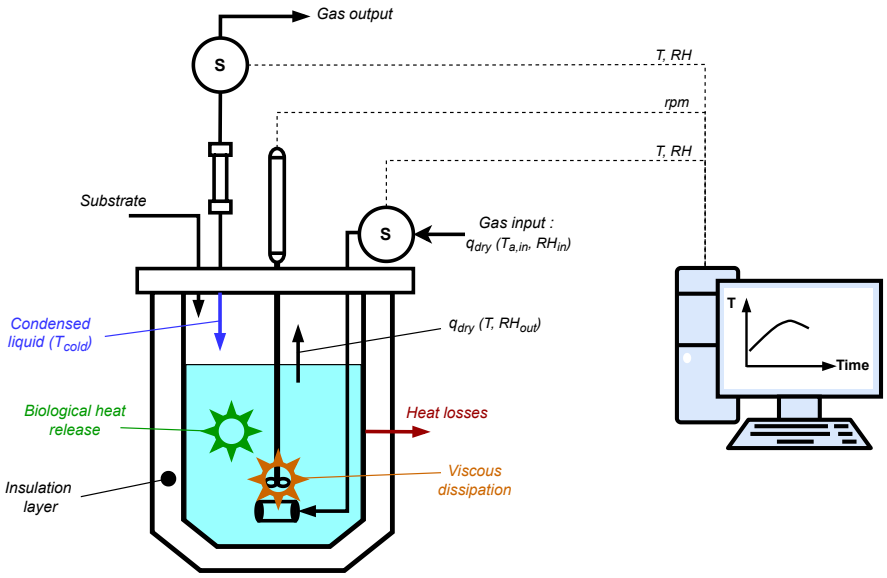

Fig. 1 Schematic representation of the insulated bioreactor indicating all the terms involved in the enthalpy balance.

It is important to note that, due to the use of an in-house insulated bioreactor that could not be autoclaved, cleaning was carried out with 70% ethanol. Additionally, to minimize the risk of bacterial contamination, each experiment began with 1 liter of preculture at 50 g/L ethanol to avoid contamination at the beginning of yeast growth. This preculture was then diluted to the required volume with YPD medium.

2.2 Analytical methods

Measurements were performed in duplicate using samples at various dilutions for all biological variables, resulting in standard deviations consistently below 5%. The values reported in the analysis represent the mean of these measurements, ensuring their precision and reliability for model implementation.

2.2.1 Yeast concentration

Yeast concentration was determined by centrifuging bioreactor samples at 2 ℃and 5800× g for ten minutes in a Centrifuge 5804 R Eppendorf, drying them in a Memmert oven at 105 ℃for seven days, and then weighing.

2.2.2 Glucose, ethanol, and glycerol concentrations

Glucose, ethanol, and glycerol concentrations were measured using high-pressure liquid chromatography (HPLC) with refractive index detection, utilizing a Thermo Scientific UltiMate 3000 with a Bio-Rad Aminex HPX-87H column. The mobile phase was 2 mM

H_2SO_4 at 0.5 mL/min, with the column at 30 ℃. Supernatants were filtered through a Whatman Spartan 0.20 μm/30 mm syringe filter before HPLC analysis.

3 Theoretical formulation

The biological formulation comes from a previous work (González-Hernández et al, 2022). In the present work, the heat of each metabolic pathway and the bioreactor global enthalpy balance were added. For the development of the rigorous enthalpy balance, capable of predicting the evolution of temperature over time, the following assumptions hold:

1. Perfectly stirred bioreactor,
2. Airflow at the saturated vapor pressure before the condenser,
3. Condensed water in the cooling system returns to the bioreactor at 10 ℃,
4. Constant viscous dissipation without considering the influence of medium properties variation throughout the fermentation process,
5. Constant heat exchange coefficient between the reactor and the surroundings.

3.1 Biological model

The anaerobic metabolic pathway (ANF) must be included in the model even under aerobic conditions (Eq. 1). During aerobic fermentation (AF) by *Saccharomyces cerevisiae* (when glucose levels exceed 0.10-0.15 g/L) (Eq. 2), the oxygen demand can surpass the available aeration capacity. This can lead to simultaneous anaerobic fermentation, as evidenced by glycerol production (Eq. 1). At lower glucose concentrations (below 0.10-0.15 g/L), yeast growths by glucose respiration (GR) (Eq. 3), shifting to ethanol respiration (ER) under aerobic conditions once glucose is depleted (Eq. 4). These intricate dynamics are addressed in the comprehensive biological model developed in a previous work (González-Hernández et al, 2022). The heat of each reaction were added in the present formulation:

$$Glc \xrightarrow{\mu_1} Y_{1X/Glc}X + Y_{1EtOH/Glc}EtOH + Y_{1Gly/Glc}Gly + \Delta H_1 \quad (1)$$

$$Glc + Y_{2O_2/Glc}O_2 \xrightarrow{\mu_2} Y_{2X/Glc}X + Y_{2EtOH/Glc}EtOH + \Delta H_2 \quad (2)$$

$$Glc + Y_{3O_2/Glc}O_2 \xrightarrow{\mu_3} Y_{3X/Glc}X + \Delta H_3 \quad (3)$$

$$EtOH + Y_{4O_2/EtOH}O_2 \xrightarrow{\mu_4} Y_{4X/EtOH}X + \Delta H_4 \quad (4)$$

The whole system of differential equations can be expressed in matrix form as the multiplication of the transpose of the stoichiometric matrix by the rate vector that includes the kinetics rates of these four metabolic pathways (R_1 to R_4) and the aeration process (R_a):

$$\frac{d}{dt}\begin{bmatrix} Glc \\ O_2 \\ EtOH \\ Gly \\ X \end{bmatrix} = \begin{bmatrix} -\frac{1}{Y_{1X/Glc}} & 0 & \frac{Y_{1EtOH/Glc}}{Y_{1X/Glc}} & \frac{Y_{1Gly/Glc}}{Y_{1X/Glc}} & 1 \\ -\frac{1}{Y_{2X/Glc}} & -\frac{Y_{2O_2/Glc}}{Y_{2X/Glc}} & \frac{Y_{2EtOH/Glc}}{Y_{2X/Glc}} & 0 & 1 \\ -\frac{1}{Y_{3X/Glc}} & -\frac{Y_{3O_3/Glc}}{Y_{3X/Glc}} & 0 & 0 & 1 \\ 0 & -\frac{Y_{4O_2/EtOH}}{Y_{4X/EtOH}} & -\frac{1}{Y_{4X/EtOH}} & 0 & 1 \\ 0 & 1 & 0 & 0 & 0 \end{bmatrix}^T \times \begin{bmatrix} R_1 \\ R_2 \\ R_3 \\ R_4 \\ R_a \end{bmatrix} \quad (5)$$

The kinetics rate expressions of the model are provided in Appendix A. It is worth mentioning that this model allows each metabolic pathway to be automatically activated or deactivated as growth conditions change (González-Hernández et al, 2022). By adding the enthalpies of reaction, this biological model can predict the contribution of each metabolic pathway to the heat power released by the biological activity:

$$q_{h,bio} = -V\left[\underbrace{\frac{R_1}{Y_{1X/Glc}}\frac{\Delta H_1}{M_{Glc}}}_{\text{ANF}} + \underbrace{\frac{R_2}{Y_{2X/Glc}}\frac{\Delta H_2}{M_{Glc}}}_{\text{AF}} + \underbrace{\frac{R_3}{Y_{3X/Glc}}\frac{\Delta H_3}{M_{Glc}}}_{\text{GR}} + \underbrace{\frac{R_4}{Y_{4X/EtOH}}\frac{\Delta H_4}{M_{EtOH}}}_{\text{ER}}\right] \quad (6)$$

3.2 Enthalpy balance

The system considered in this balance is the liquid present in the bioreactor, whose temperature is simply denoted as T. The heat capacity of the liquid is supposed to be the same as that of liquid water. The overall enthalpy balance links the time change of the system enthalpy to the heat generated by the biological activity and the physical exchanges. The latter include thermal losses, viscous dissipation, the heat required to heat the airflow and the latent heat of vaporization needed to saturated this airflow. The temperature (T_{in}) and relative humidity (RH_{in}) of the aeration air flow of aeration entering the bioreactor are measured during the process by the Sensirion sensor. The gas is expected to separate from the liquid at the temperature of the liquid and saturated vapor pressure. Then, the cold finger changes this enthalpy before the gas flow leaves the reactor but does not affect the system enthalpy. Besides, condensed water returns to the system at the cold finger temperature. This system is schematized in figure 1.

The air enthalpy used classical references for zero enthalpy (air at 0°C and liquid water at 0°C). The rigorous expressions of the enthalpy fluxes should involve the flow rate of the dry gas (air or nitrogen), as this is a constant value at steady-state, despite the change of vapor content (evaporation or condensation). This quantity also ensures the additivity of gas and vapor enthalpies when using the absolute moisture content of the gas ($Y = \rho_v/\rho_{dry}$). The complete balance finally reads as follows:

$$\frac{d(\rho_\ell V h_\ell)}{dt} = q_{h,bio} + q_{h,visc} - q_{h,loss} + q_{h,aeration} + q_{h,cond} \tag{7}$$

Where the enthalpy fluxes read as:

$$q_{h,loss} = A h_h (T - T_{ext}) \tag{8}$$
$$q_{h,aeration} = q_{dry}(h_{dry,in} - h_{dry,out}) \tag{9}$$
$$q_{h,cond} = q_{\ell,cond} h_{\ell,T_{cold}} \tag{10}$$

With the following expressions for the the mass fluxes and the specific enthalpies:

$$q_{dry} = F \rho_{dry} \tag{11}$$
$$q_{\ell,cond} = q_{dry}(Y_{out} - Y_{cold}) \tag{12}$$
$$h_{dry,in} = C_{pa} T_{in} + Y_{in}(C_{pv} T_{in} + L_v^0) \tag{13}$$
$$h_{dry,out} = C_{pa} T + Y_{out}(C_{pv} T + L_v^0) \tag{14}$$
$$h_{\ell,T_{cold}} = C_{p\ell} T_{cold} \tag{15}$$

In equation (12), Y_{out} and Y_{cold} are computed assuming the air to be fully saturated, respectively at temperatures T and T_{cold}.

The time derivative of the system enthalpy can be developed to distinguish the effects of temperature change and volume change:

$$\frac{d(\rho_\ell V h_\ell)}{dt} = \rho_\ell V C_{p\ell} \frac{dT}{dt} + \rho_\ell C_{p\ell} T \frac{dV}{dt} \tag{16}$$

Where the volume variation is negative, equal to the evaporation flux due to aeration:

$$\rho_\ell \frac{dV}{dt} = q_{dry}(Y_{in} - Y_{out}) \tag{17}$$

See Appendix B for further detail of this enthalpy balance.

3.3 Model calibration

3.3.1 Heat balance without yeast

The physical parameters of the bioreactor were obtained by inverse analysis using experiments without biological activity. For this purpose, a data set was generated under different operation conditions –without stirring, with and without aeration(Table 1) –to isolate the phenomena in which the desired physical parameter is involved as far as possible. This greatly simplifies the energy balance, reduces interference from other processes in the measurement,which increases accuracy. Therefore, the overall energy balance (Eq. 7) can be simplified:

$$\frac{d(\rho_\ell V h_\ell)}{dt} = -q_{h,loss} + q_{h,aeration} + q_{h,cond} \tag{18}$$

The same operating conditions of the fermentation process were used (initial temperature, aeration intensity, etc.), where only the substrate and culture medium without yeast inoculation were employed, and therefore, the yeast activity was excluded from the model. A mixture of antibiotic (streptomycin at 400 μg/mL and, penicillin at 135 μg/mL) and antifungal (amphotericin B at 2.5 μg/mL) products was added to the bioreactor to avoid contamination.

Table 1 Experiments carried out for the estimation of the physical parameters of the heat balance without yeast activity.

Experiment	Aeration	Stirring	Initial temperature (°C)	V (mL)
I	no	no	35	4344
II	yes	no	35	4344

Firstly, the external heat transfer coefficient was determined without agitation or aeration (Experiment I). Next, only aeration was activated (Experiment II) to validate the heat balance due to the airflow (enthalpy balance involving both the sensible and latent heat).

3.3.2 Heat balance with yeast activity

The biological heat for each metabolic pathway involved under complete anaerobic or aerobic conditions were progressively estimated by inverse analysis. For this purpose, five batch fermentation experiments (A to E) were conducted under various operating conditions to generate representative data and distinguish the phenomena considered in the model (different initial glucose, ethanol, and yeast concentrations, and oxygen availability (Table 2)) (González-Hernández et al, 2022). By varying the initial concentrations and oxygen availability in the system, we can produce different perturbations involving all parameters to be estimated. This approach is required to avoid over-parametrization during the fitting process (González-Hernández and Perré, 2024). Contrary to experiments A to D, experiment E was carried out without gas injection. This set of experiments allowed the different metabolic pathways to vary in importance and time, which was required to identify the four heats of reaction.

Table 2 Initial conditions of batch fermentation experiments performed under anaerobic and aerobic conditions

Experiment	O_2 (mg/L)	Glc (g/L)	$EtOH$ (g/L)	Gly (g/l)	X (g/L)	T (°C)	V (mL)
A (Anaerobic)	-	15.37	10.60	0.12	0.30	25.20	4365
B (Anaerobic)	-	31.06	10.99	0.15	0.81	26.50	4075
C (Aerobic)	5.84	15.93	9.11	0.10	0.50	26.10	4242
D (Aerobic)	2.86	30.79	9.84	0.25	1.31	25.20	3309
E	-	12.41	1.27	0.15	0.40	23.80	4279

3.3.3 Parameter estimation

Inverse analysis is based on a fitness function designed to quantify the difference between predicted and measured values. When several metabolic pathways coexist, the determination of unknown parameters becomes complex and must be carried out on several tests simultaneously. In this case, the fitness function must include several tests ($\ell = 1...L$):

$$fitness = \frac{1}{LN} \sum_{\ell=1}^{L} \sum_{i=1}^{N} \left| \frac{T_{e(i)}^{(\ell)} - T_{m(i)}^{(\ell)}}{T_{e,max}^{(\ell)} - T_{e,min}^{(\ell)}} \right| \tag{19}$$

where $T_{e(i)}^{(\ell)}$ is the experimental temperature of experiment ℓ at time t_i and $T_{m(i)}^{(\ell)}$ is the corresponding model output data. $T_{e,max}^{(\ell)}$ and $T_{e,min}^{(\ell)}$ are the maximum and minimum experimental temperature values registered during experiment ℓ.

The model was implemented in Python using SciPy *solve_ivp* function for solving the ODE system with the LSODA integration method. Calibration was done with Particle Swarm Optimization (PSO) from the PySwarm package, with specific parameter values for faster convergence. Parameter ranges were defined based on literature values. The uniqueness of the optimization solution was validated by the very low standard deviation values observed between ten iterations in each calibration process, which were computed using the *std* function from Numpy.

3.3.4 Statistical analysis

In this study, the mean relative error was employed as metric to assess the accuracy of the fitting process. The MRE for a single variable across multiple data points N is mathematically expressed as:

$$MRE = \frac{1}{N} \sum_{i=1}^{i=N} \left| \frac{y_{e(i)} - y_{m(i)}}{y_{e(i)}} \right|, \tag{20}$$

To evaluate the overall fidelity of the model across all experimental conditions M and variables L, we introduced the global mean relative error (GMRE). The GMRE provides a holistic measurement of the model's fitting performance and is defined as:

$$GMRE = \frac{1}{ML} \sum_{k=1}^{M} \sum_{j=1}^{L} MRE_{(j)}^{(k)}, \tag{21}$$

where $y_{e(i)}$ is the experimental data value $-i$ of the variable $-j$ (Glc, $EtOH$, Gly, X, and T) in experiment $-k$, and y_m is the model output data value $-i$ of the variable $-j$ in experiment $-k$.

4 Results and discussion

4.1 Estimation of global heat transfer coefficient

As previously explained, the global heat exchange coefficient to account for heat losses from the insulated bioreactor to the environment was estimated through inverse analysis. This was done using the enthalpy heat balance model without biological activity and the experimental data generated without stirring nor aeration (Experiment I, Table 1). The global heat transfer coefficient was estimated at 0.74 $\pm$0.00 W/K/m^2(SD $\approx 10^{-7}$). As seen in Fig. 2a, the heat balance model perfectly fits the bioreactor temperature (mean relative error of 0.44 %).

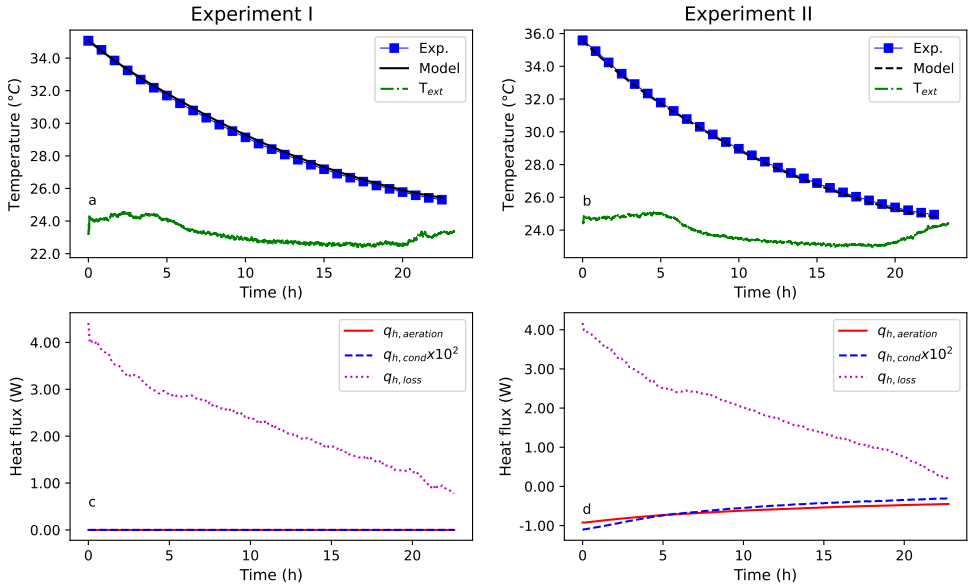

Fig. 2 Simultaneous temperature fitting to estimate the physical heat exchange without (a) and with (b) aeration (experiments I and II, respectively). Respective contributions of the heat demands due to thermal losses and aeration (c,d) (T_{ext}: Temperature of laboratory room (°C), $q_{h,aeration}$: Heat power associated with aeration (W), $q_{h,cond}$: Heat power associated with condensation (W)), and $q_{h,loss}$: Heat power losses to the environment (W)).

In Experiment II, aeration was added to thermal losses without stirring. As the enthalpy balance on air is completely determined by measured data (relative humidity and T) and by the assumption on condensation (Eqs. 9 and 10), no further parameter needed to be fitted. Hence, the prediction of Experiment II by the model using the parameter fitted in Experiment I (the global heat exchange coefficient to the environment) serves here as validation. Fig. 2b shows how the model effectively characterizes the temperature profile under these varying conditions, exhibiting a mean relative error of only 0.41 %. This outcome confirms the model's reliability and corroborates

the accuracy of the value found for the global heat exchange coefficient. As can be seen in figures 2c and 2d, heat losses from the bioreactor to the environment and evaporation associated with the aeration process are the main contributors to heat losses in the system.

4.2 Heat of reaction for complete anaerobic conditions

Under completely anaerobic conditions, a unique metabolic pathway is activated in the biological model (Eq. 1), since the aerobic processes are automatically deactivated in the mechanistic model due to the absence of oxygen. The biological model, with its reaction enthalpies, was coupled with the heat balance model to predict the temperature evolution. Using this combined model, the biological heat release and the heat generation due to viscous dissipation were estimated using inverse analysis combining experiments A and B. The viscous dissipation rate was found to be 0.97 ± 0.00 W (SD $\approx 10^{-4}$) and the fitting process resulted in biological enthalpies of ΔH_1=-101.28 ± 0.02 kJ/mol of glucose, which falls well within the reported literature range of -71.5 to -119.2 kJ/mol of glucose (Williams, 1982). The low standard deviation values demonstrate the results quality and the relevance of the combined model. The model was able to reproduce temperature data with mean relative errors of 0.28 and 0.21 % for experiments A and B, respectively. Fig. 3 illustrates the simultaneous temperature fitting to estimate viscous dissipation and metabolic heat release under various completely anaerobic conditions. Additionally, it displays the individual contribution of each heat exchange process.

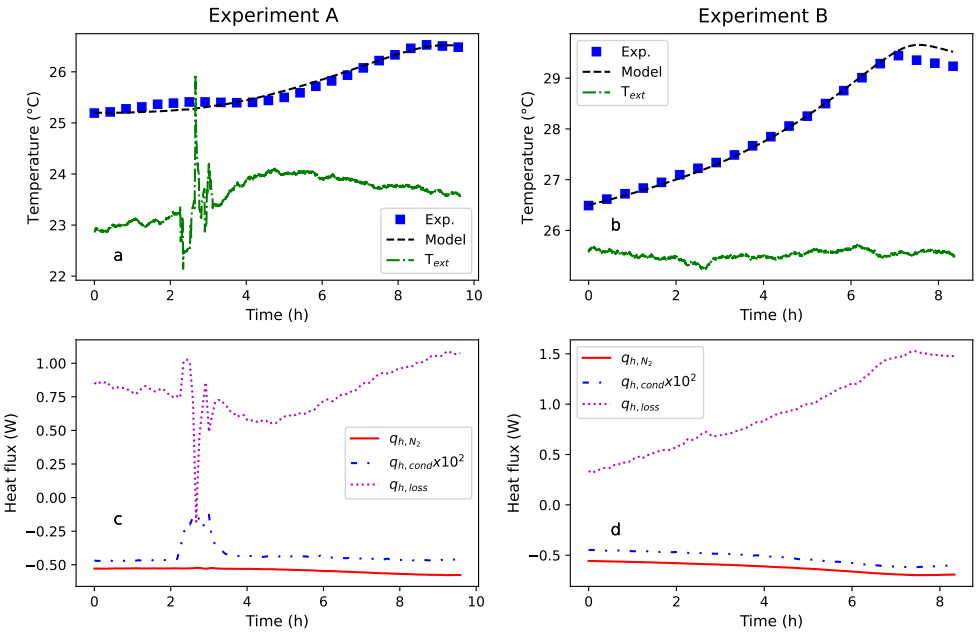

Fig. 3 Simultaneous temperature fitting to estimate viscous dissipation and metabolic heat release under different completely anaerobic conditions (a,b). Individual heat losses related to the insulated bioreactor (c,d) (T_{ext}: Temperature of laboratory room (°C), $q_{h,N2}$: Heat power associated with nitrogen injection (W), $q_{h,cond}$: Heat power associated with condensation (W), and $q_{h,loss}$: Heat power losses to the environment (W)).

In Fig. 3a, while the temperature predictions are generally accurate, minor discrepancies with the experimental data arise in the first six hours. The abrupt changes in the external temperature recorded by the sensor are due to sunlight through the glass windows of the experimental room, and the inability of the model to account for a transient state inside the insulation (Eq. 8). Figure 4 depicts the evolution of glucose concentration and power released with the identified heat of reaction for experiments A and B. In both cases, the biological model predicts nicely the experimental kinetics of glucose consumption (9.76 and 17.44%, respectively (González-Hernández et al, 2022)). It is important to remark that the power magnitudes of the physical effects (Figs. 3c and 3d) are lower than those of the biological activity (Figs. 4a and 4b), making a modest contribution to the overall enthalpy balance. This observation guarantees the relevance of the information used to determine the heat released by biological activity.

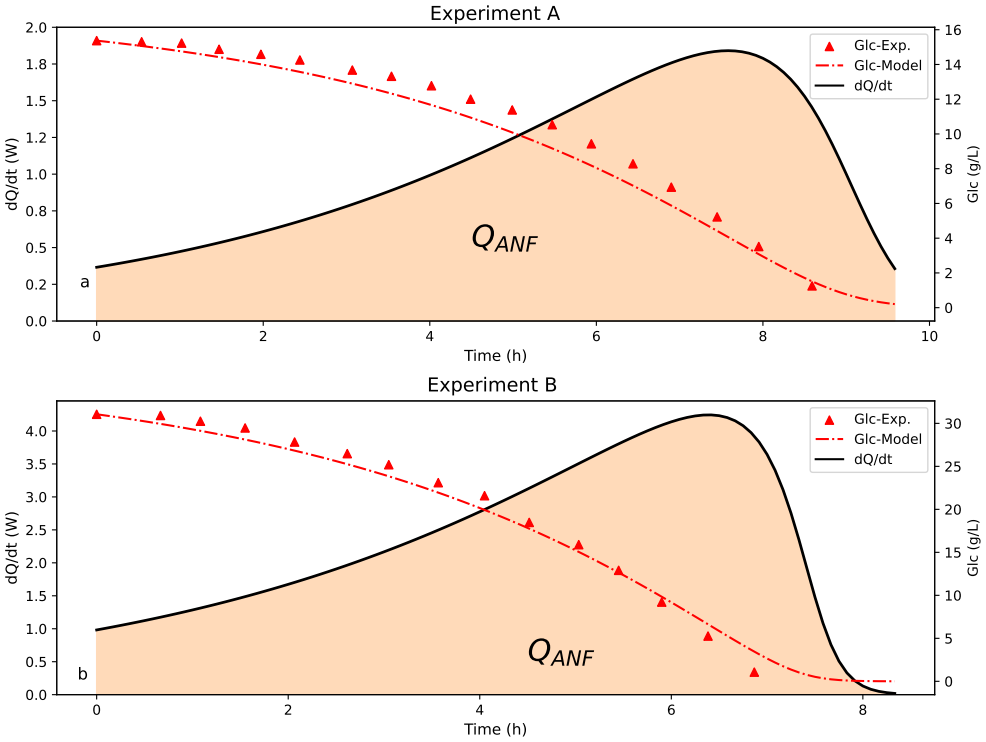

Fig. 4 Overall biological heat released over time of experiments A and B (Q: Biological heat released (J), Glc: Glucose (g/L), and ANF: Anaerobic fermentation)

.

Although the model calibration demonstrates good accuracy in predicting the temperature inside the bioreactor, it is worth noting that they may be influenced by error propagation from the biological model. However, it's important to highlight that the latter is quite accurate, reporting a global mean relative error in the most important variables of the system (glucose, yeast, ethanol and glycerol concentrations) of 6.84% (González-Hernández et al, 2022). It is also important to consider that viscous dissipation is influenced by the density and viscosity of the mixture, which changes over time, while it was assumed constant in the model. In practice, viscous dissipation decreases with the consumption of reagents like glucose while ethanol, less viscous than glucose, and yeast are produced concurrently. While an elevated yeast concentration might imply an increased viscosity, its very low volumetric concentration between 2.06 and 6.50 g/L at the end of the experiments (González-Hernández et al, 2022) cannot counterbalance the substitution of glucose for ethanol. Indeed, the glucose consumption rate exceeds the production rate of ethanol, by a factor roughly equal to 2.5 (see figure 6), which in turn is higher than the yeast formation rate. Concerning the heat balance model, the most significant heat losses were due to heat losses to the environment and

evaporation associated with gas injection, confirming the results obtained previously in section 4.1.

Temperature profiles can serve as indicators of metabolism. As evidenced in Figs. 3a and 3b, both temperature profiles exhibit two phases: an exponential increase in temperature over time corresponding to anaerobic fermentation, followed by a declining temperature phase indicating glucose depletion. Temperature, as the sole parameter, does not immediately allow for a precise distinction of phase transitions. Nevertheless, the rate of temperature change is directly tied to the metabolic heat release (dQ/dt), which offers immediate insights into the process kinetics, indicating substrate limitation and progressive ethanol inhibition. Furthermore, as one unique pathway is active here, the total power generated Q_{ANF} offers information on the process stoichiometry. Indeed, glucose consumption is derived from the following relationship:

$$Glc = \frac{M_{Glc} Q_{ANF}}{V \Delta H_1} \tag{22}$$

where:

$$Q_{ANF} = \int_{t_0}^{t} (dQ_1/dt) dt \tag{23}$$

Similarly, crucial metabolites like ethanol and yeast concentration can be determined by knowing the corresponding stoichiometric yields in advance:

$$EtOH = Y_{1EtOH/Glc} Glc \tag{24}$$

$$X = Y_{1X/Glc} Glc \tag{25}$$

Finally, it is essential to remark that extending the biological model to encompass the heat balance introduces temperature as a new, easy-to-measure, parameter with a great potential in process control.

4.3 Heats of reaction under aerobic conditions

Modeling the temperature behavior under aerobic conditions is more complex due to the involvement of several metabolic pathways. For example, the anaerobic pathway can coexist with aerobic metabolism when the oxygen demand exceeds the oxygen supplied by aeration. Consequently, under these conditions, the direct determination of the enthalpy of individual metabolic pathways under aerobic conditions is inherently challenging. To overcome this problem, the inverse procedure was carried out simultaneously on a set of two experiments (Experiments C and D).

Thanks to the similarity in culture conditions regarding chemical and biological compositions between aerobic and anaerobic conditions, we employed the previously obtained physical parameters (thermal losses, viscous dissipation). It is important to note that, due to the Crabtree effect, glucose respiration is a metabolic pathway activated only during a very short time by the mechanistic model. Considering that our experimental information is the temperature level, an integrator of the heat flux, this short time is not enough to get accurate experimental information. This mathematical

degree of freedom could then be used misleadingly in optimization. To avoid over-parametrization, the enthalpy of glucose respiration was not fitted but taken from literature: ΔH_3 = -1490.40 kJ per mole of glucose, as reported by Volesky et al (1982).

This allowed the inverse analysis to focus on reaction enthalpies poorly documented in literature: glucose aerobic fermentation and ethanol respiration. Fig. 5 shows the simultaneous temperature fitting for estimating individual metabolic heat under different aerobic conditions. The time evolution of the individual contributions of each heat exchange process and the respective contributions of each metabolic pathway are plotted in separate graphs (Fig. 6).

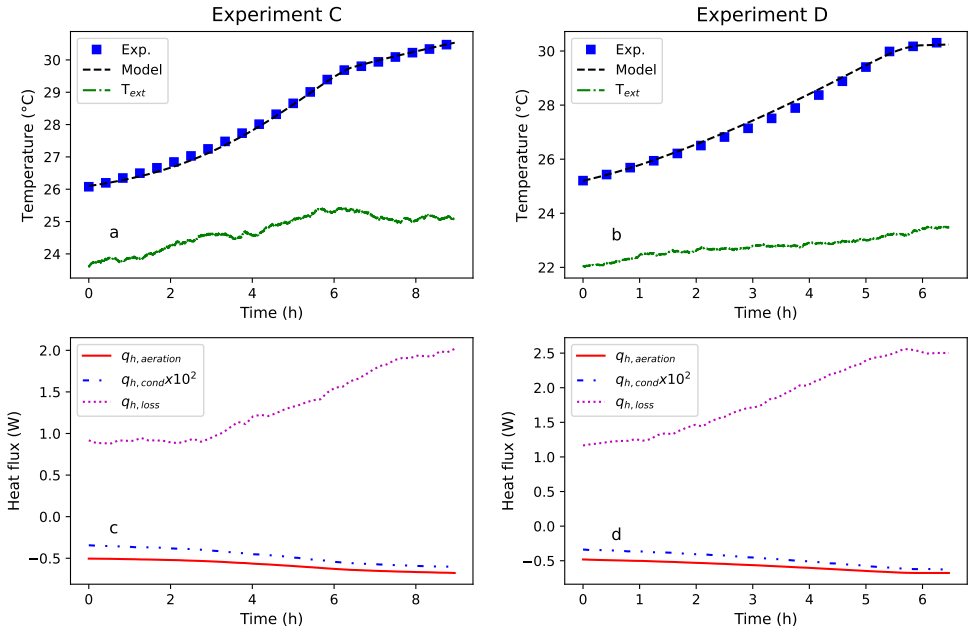

Fig. 5 Simultaneous temperature fitting for estimating individual metabolic heat release under different aerobic conditions (a,b). Individual heat losses related to the insulated bioreactor (c,d) (T_{ext}: Temperature of laboratory room (°C), $q_{h,aeration}$: Heat power associated with aeration (W), $q_{h,cond}$: Heat power associated with condensation (W), and $q_{h,loss}$: Heat power losses to the environment (W)).

The optimization process rapidly and effectively converged to a value of ΔH_2 =-231.27±0.06 kJ/mol of glucose, and ΔH_4 =-662.94±0.54 kJ/mol of ethanol, with mean relative errors of 0.24 and 0.38% for experiment C and D, respectively. The value obtained for the heat of reaction in aerobic fermentation (ΔH_2) is consistent with the findings of Volesky et al (1982); Auberson and Von Stockar (1992), as it is lower than that for aerobic respiration (ΔH_3). The obtained results validate the heat balance model developed in this study while confirming the quality of the biological

model (González-Hernández et al, 2022). Once again, the biological model exhibits remarkable precision, reporting a global MRE of 10.39 % under aerobic conditions.

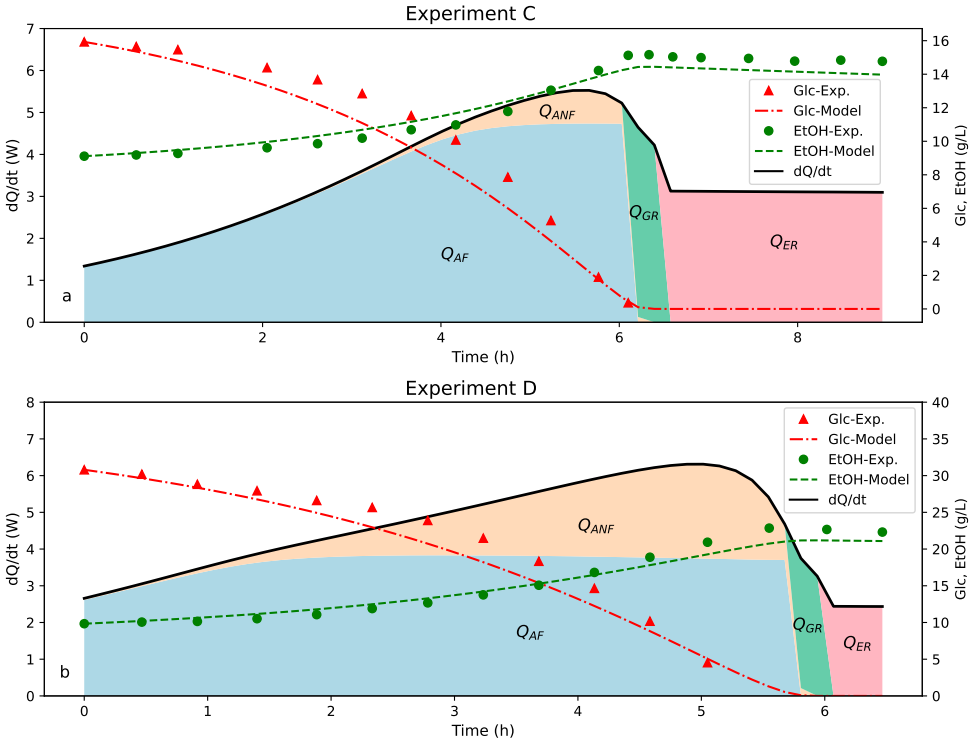

Fig. 6 Distinct contributions of various metabolic pathways to the overall biological heat released over time of experiments C and D (Q: Biological heat released (J), Glc: Glucose (g/L), EtOH: Ethanol (g/L), ANF: Anaerobic fermentation, AF: Aerobic fermentation, GR: Glucose respiration, and ER: Ethanol respiration)

.

Similarly to all previous tests, heat losses to the environment and latent heat of evaporation are the major contributors to the total heat loss (Figs. 5c and 5d). In both experiments, the heat released by the biological activity, shared among all active metabolic pathways with a predominance of aerobic fermentation, is much higher than the flux magnitude of the physical effects. Again, the temperature information is mainly tied to the biological activity, which explains the success of our identification procedure. In experiment C (Fig. 6a), the contribution of the anaerobic metabolic pathway is lower than in experiment D (Fig. 6b). This is explained by higher oxygen consumption due to a greater yeast concentration for the same oxygen input through aeration (González-Hernández et al, 2022). Under these conditions, due to the coexistence of metabolic pathways, the use of the metabolic heat released to establish stoichiometric relationships to estimate glucose consumption is more complex. As can

be seen in Figs. 6a and 6b, the metabolic heat generated depends on the activity of each metabolic pathway. The glucose consumption under these conditions can be calculated as follows:

$$Glc = \frac{M_{Glc}}{V}\left(\frac{Q_{ANF}}{\Delta H_1} + \frac{Q_{AF}}{\Delta H_2} + \frac{Q_{GR}}{\Delta H_3}\right) \tag{26}$$

where:

$$Q_{ANF} = \int_{t_0}^{t} (dQ_1/dt)dt \tag{27}$$

$$Q_{AF} = \int_{t_0}^{t} (dQ_2/dt)dt, \tag{28}$$

$$Q_{GR} = \int_{t_0}^{t} (dQ_3/dt)dt, \tag{29}$$

Similarly, the determination of ethanol and yeast concentration needs the prior knowledge of the corresponding stoichiometric yields:

$$EtOH = \frac{M_{Glc}}{V}\left(Y_{1EtOH/Glc}\frac{Q_{ANF}}{\Delta H_1} + Y_{2EtOH/Glc}\frac{Q_{AF}}{\Delta H_2}\right) \tag{30}$$

$$X = \frac{M_{Glc}}{V}\left(Y_{1X/Glc}\frac{Q_{ANF}}{\Delta H_1} + Y_{2X/Glc}\frac{Q_{AF}}{\Delta H_2} + Y_{3X/Glc}\frac{Q_{GR}}{\Delta H_3}\right) \tag{31}$$

The estimation of the stoichiometry of the process, as stated in Eqs. 26-31, requires the respective contributions of the individual metabolic heats. This is almost impossible in the presence of several coexisting metabolic pathways, as only the total metabolic heat can be measured. In these circumstances, modeling can take advantage of total metabolic heat as a new measurable response variable, together with substrate and product concentrations that can be measured online (e.g., by Raman spectroscopy for substrate and metabolite concentration (Yang et al, 2024)).

On the other hand, considering the precision and robustness of the model, it could be utilized as a tool to design specific processes, for example aiming to avoid or promote concurrent metabolic pathways, not only for Crabtree-positive yeasts but also for Crabtree-negative yeasts. The temperature profile, once again, demonstrates its utility as a qualitative metabolic indicator, showing an initial exponential temperature increase followed by a slight decline with glucose depletion, transitioning into a linear growth behavior corresponding to ethanol respiration. It is noteworthy that, for the first time in the literature, such an extensive model is reported, encompassing the prediction of temperature over time, including the ethanol respiration process.

4.4 Model training in a feedback application

As possible application of the complete model, we propose here an example of online training. For that purpose, we used experiment E performed without gas injection. The headspace is just connected to the environment through filters. Despite the absence of aeration, oxygen present in the headspace of the bioreactor is transferred to the

liquid phase to support biological processes (with a specific rate of $2.10^{-4}s^{-1}$, previously estimated by La et al (2020) for the same experimental setup). This transfer is due to the gap of oxygen activity resulting from the biological consumption of dissolved oxygen and promoted by agitation. Consequently, aerobic and anaerobic metabolic pathways are activated simultaneously (Fig. 7d). However, the extent of aerobic metabolism is significantly reduced due to oxygen limitations primarily caused by the absence of aeration and the low transfer rate of oxygen (2.10^{-4} s^{-1}) from the bioreactor headspace to the yeast medium. The presence of bubbles due to aeration lowers the apparent viscosity of the fluid. Consequently, the viscous dissipation obtained in the previous experiments (A to D) underestimates the viscous dissipation in experiment E. The temperature prediction using the previous dissipation value (initial guess) underestimates the temperature (Fig. 7b).

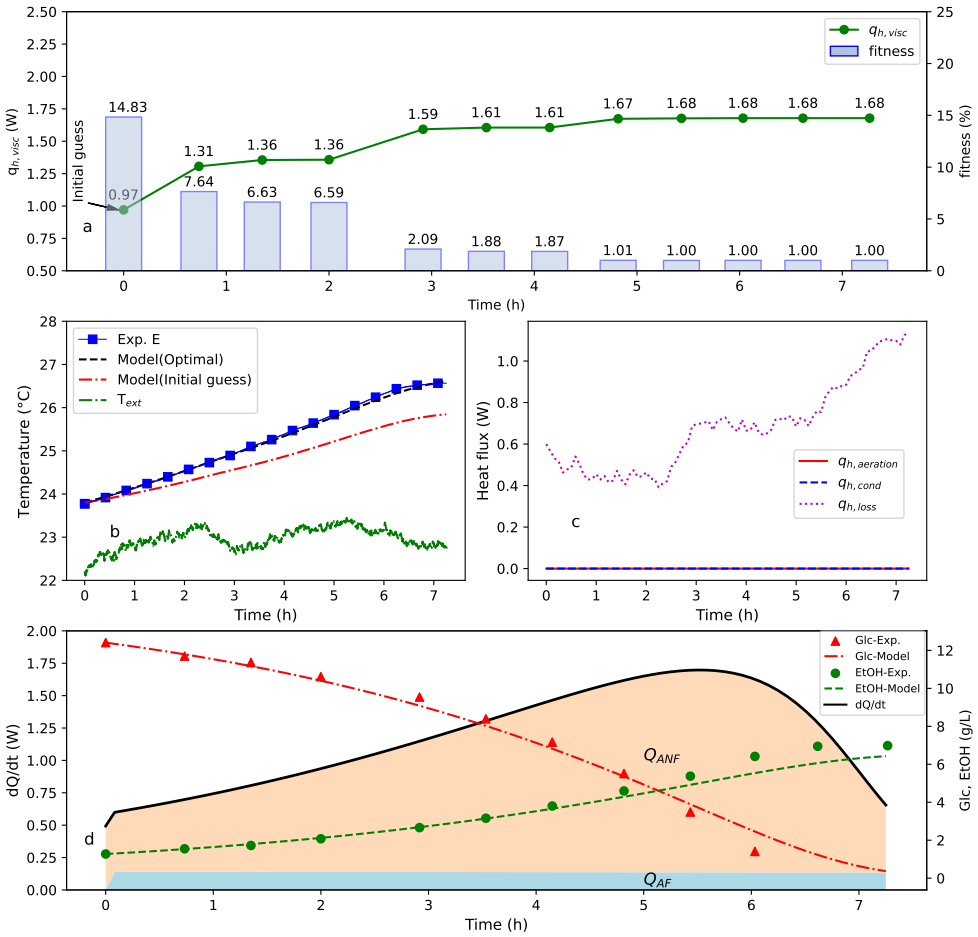

Fig. 7 Estimating viscous dissipation over time for experiment E (without aeration) by training the model over an increasing time range (a). Comparison between experimental data and model predictions for the initial guess (0.97W) of viscous dissipation and the optimum value obtained by online training (1.68W)(b). Individual heat losses related to the insulated bioreactor (c) and the distinct contributions of various metabolic pathways to the overall biological heat released over time (d) (Q: Biological heat released (J), T_{ext}: Temperature of laboratory room (°C), $q_{h,visc}$: Heat power of viscous dissipation (W), $q_{h,aeration}$: Heat power associated with aeration (W), $q_{h,cond}$: Heat power associated with condensation (W), and $q_{h,loss}$: Heat power losses to the environment (W), Glc: Glucose (g/L), EtOH: Ethanol (g/L), ANF: Anaerobic fermentation, and AF: Aerobic fermentation). An animated presentation of this online training is available as supplementary information.

Unlike the approach used in experiments A to D, the model validation in this instance employed a progressive training process, demonstrating the model can be trained during a process for better control/command (Fig. 7a). The training process is focused on the viscous dissipation coefficient through an optimization process using the PSO method. Using the previous value of viscous dissipation as initial guess, the

first instants of the process ([t_0, t_i]) are used to adapt the parameter, progressively increasing the number of experimental points as the time advances. Therefore, the training process reliability and thoroughness increase over time.
The quality of the training process is supported by consistently low standard deviation values (SD<10^{-3}W) observed throughout the optimization of each expanded range over time. The best fitted value using the complete data set gives a viscous dissipation coefficient of 1.68±0.00 W (SD ≈ 10^{-4}), achieving to predict the temperature inside the bioreactor with a mean relative error of 0.13%. Fig. 7a shows that the fitted value of viscous dissipation for online training is stabilized after approximately 3 hours, suggesting that even a modest amount of experimental data is adequate for accurate predictions (an animation of this procedure is proposed as Supplementary Material). After this period, could be expected that the model is accurate enough for control/command. This characteristic highlights the potential of a mechanistic model of the metabolic pathways coupled with a comprehensive enthalpy balance for process control with online tuning. The measured temperature is first used to tune the model and then to control the process, for example to trigger flushing in a fed-batch reactor or to know when the process can be stopped. In industrial plants, the heat power needed to control temperature can be used instead of temperature. Thanks to a relevant mechanistic model, readily collected information could be used effectively to control the process. Finally, it is important to note that while estimating viscous dissipation through fitting during the validation process may be seen as a limitation. However, it also offers a significant advantage by enabling indirect estimation of the parameter using the model. This aspect should be addressed in future studies to further improve the model's robustness.

5 Conclusions

This study introduces a comprehensive model of yeast that combines the main metabolic pathways of *Saccharomyces cerevisiae*, including the heats of reaction, and a rigorous enthalpy balance of the bioreactor. Using an insulated bioreactor in combination with a mechanistic model, the individual metabolic heat was determined for the first time: -101.28±0.02kJ/mol for anaerobic fermentation, -231.27±0.06kJ/mol for aerobic fermentation, and -662.94±0.54kJ/mol for ethanol respiration. The model was calibrated and validated, accurately predicting bioreactor temperature for anaerobic and aerobic conditions (MRE below 0.38%). The viscous dissipation is a key parameter specific to the bioreactor and the growth conditions. However, we demonstrated that this parameter could be fitted accurately from the early stages of the experiment for further prediction of the remaining part. This allows temperature, or the power needed to maintain temperature, to be introduced as a measurable response variable, improving model calibration and control potential.

Supplementary information. An animated presentation of the online training process in a feedback application is available as supplementary information.

Acknowledgements. Communauté Urbaine du Grand Reims, Département de la Marne, Région Grand Est and European Union (FEDER Champagne-Ardenne

2014-2020, FEDER Grand Est 2021-2027) are acknowledged for their financial support to the Chair of Biotechnology of CentraleSupélec and the Centre Européen de Biotechnologie et de Bioéconomie (CEBB).

CRediT author statement. YGH: Conceptualization, Methodology, Formal analysis, Modeling, Visualization, Writing-Original draft preparation, Writing–Reviewing and Editing. EM: Investigation, Methodology. PP: Conceptualization, Methodology, Formal analysis, Modeling, Visualization, Writing–Reviewing and Editing, Supervision, Funding acquisition.

Funding. This study was funded by Communauté Urbaine du Grand Reims, Département de la Marne, Région Grand Est and European Union (FEDER Champagne-Ardenne 2014-2020, FEDER Grand Est 2021-2027).

Declarations

Ethical approval. Not applicable.

Consent for publication. Not applicable.

Competing interest. The authors declare no competing interests.

Appendix A Additional information of biological model

Anaerobic fermentation process based on glucose

$$R_1 = \mu_{max1} M_{(Glc)} I_{(O_2)} I_{(EtOH)} X \tag{A1}$$

Aerobic fermentation process based on glucose

$$R_2 = \mu_{max2} \lambda_f M_{(Glc)} M_{(O_2)} I_{(EtOH)} X \tag{A2}$$

Respiration process based on glucose

$$R_3 = \mu_{max3} (1 - \lambda_f) M_{(Glc)} M_{(O_2)} I_{(EtOH)} X \tag{A3}$$

Respiration process based on ethanol

$$R_4 = \mu_{max4} M_{(EtOH)} M_{(O_2)} I_{(Glc)} I_{(EtOH)} X \tag{A4}$$

where:

$$M_{(S)} = \frac{S}{K_{S,j} + S} \tag{A5}$$

$$I_{(S)} = \frac{K_{S,j}^{inh}}{K_{S,j}^{inh} + S} \tag{A6}$$

$M_{(S)}$ is the Monod limiting expression for substrate S, while $I_{(S)}$ is the Monod-variant inhibiting expression for substrate S. $K_{S,j}$ is the half-mean saturation coefficient for substrate S under anaerobic ($j = Ax$) or aerobic ($j = Ox$) conditions, while $K_{S,j}^{inh}$ is the half-mean saturation coefficient for substrate S inhibition under anaerobic ($j = Ax$) or aerobic ($j = Ox$) conditions.

$$\lambda_f = \frac{1}{2}\{1 + tanh[\alpha(Glc/Glc_c - 1)]\} \tag{A7}$$

λ_f is the function used for describing the transition between glucose fermentation to respiration, Glc_c is the glucose concentration value at which the transition takes place, and the α parameter, determines the sharpness of this transition. For this instance, the values of $\alpha = 150$ and Glc_c=0.125 g/L, as well as the stoichiometric and kinetic parameters of the biological model, were taken from González-Hernández et al (2022).

Aeration process

$$R_5 = k_L a(O^*_{2(T)} - O_2) \tag{A8}$$

where:

$k_L a$ is the overall oxygen transfer rate (h^{-1}) and $O^*_{2(T)}$ is the oxygen saturation value at temperature T.

Appendix B Additional information on the enthalpy balance of the bioreactor

The absolute vapor content of the air are respectively equal to:

$$Y_{in} = \frac{RH_{in} P_{sv(T_{a,in})} M_v}{P_{atm} M_a} \tag{B9}$$

$$Y_{out} = \frac{P_{sv(T)} M_v}{P_{atm} M_a} \tag{B10}$$

$$Y_{cold} = \frac{P_{sv(T_{cold})} M_v}{P_{atm} M_a} \tag{B11}$$

The latent heat of vaporization for water (kJ/kg) was assumed to vary linearly with temperature between 0 °C and 100 °C. In this linear relation, the temperature is in °C:

$$L_{v(T)} = 2503.0 - 2.46\,T \tag{B12}$$

The saturation vapor pressure of water in Pascal (N/m^2) was estimated using the following correlation, where the temperature is the absolute temperature (K)(Sonntag, 1990; Crétinon and Blanquart, 2007):

$$\begin{aligned} ln(P_{sv}(T)) = &-6096.9385\,T^{-1} + 21.2409642 - 2.711193.10^{-2}\,T \\ &+ 1.673952.10^{-5}\,T^2 + 2.433502\,ln(T) \end{aligned} \tag{B13}$$

The following physical values were supplied to the code: $C_{p\ell} \approx C_{pw}$=4184 J/(kg K), C_{pN_2}=1040 J/(kg K), C_{pa}=1005 J/(kg K), M_{N_2}=28.10^{-3} kg/m^3, M_v=18.10^{-3} kg/m^3, M_a = 29.10^{-3} kg/m^3 and A=0.50 m^2.

References

Auberson LC, Von Stockar U (1992) A unified stoichiometric model for oxidative and oxidoreductive growth of yeasts. Biotechnology and bioengineering 40(10):1243–1255

Biener R, Steinkämper A, Hofmann J (2010) Calorimetric control for high cell density cultivation of a recombinant escherichia coli strain. Journal of biotechnology 146(1-2):45–53

Biener R, Steinkämper A, Horn T (2012) Calorimetric control of the specific growth rate during fed-batch cultures of saccharomyces cerevisiae. Journal of biotechnology 160(3-4):195–201

Claes J, Van Impe J (2000) Combining yield coefficients and exit-gas analysis for monitoring of the baker's yeast fed-batch fermentation. Bioprocess Engineering 22:195–200

Crétinon B, Blanquart B (2007) Air humide-Notions de base et mesures. Techniques de l'Ingénieur, Editions TI—

Duboc P, Cascão-Pereira LG, Stockar Uv (1998) Identification and control of oxidative metabolism in saccharomyces cerevisiae during transient growth using calorimetric measurements. Biotechnology and bioengineering 57(5):610–619

González-Hernández Y, Perré P (2024) Building blocks needed for mechanistic modeling of bioprocesses: A critical review based on protein production by cho cells. Metabolic Engineering Communications p e00232

González-Hernández Y, Michiels E, Perré P (2022) A comprehensive mechanistic yeast model able to switch metabolism according to growth conditions. Fermentation 8(12):710

Guo Q, Peng QQ, Li YW, et al (2023) Advances in the metabolic engineering of saccharomyces cerevisiae and yarrowia lipolytica for the production of β-carotene. Critical Reviews in Biotechnology pp 1–15

Ingledew W, Lin YH (2011) 3.05 - ethanol from starch-based feedstocks. In: Moo-Young M (ed) Comprehensive Biotechnology (Second Edition), second edition edn. Academic Press, Burlington, p 37–49

La A, Du H, Taidi B, et al (2020) A predictive dynamic yeast model based on component, energy, and electron carrier balances. Biotechnology and Bioengineering 117(9):2728–2740

Lee J, Lee SY, Park S, et al (1999) Control of fed-batch fermentations. Biotechnology advances 17(1):29–48

Maskow T, Schubert T, Wolf A, et al (2011) Potentials and limitations of miniaturized calorimeters for bioprocess monitoring. Applied Microbiology and Biotechnology 92:55–66

Nya E, Etukudo O (2023) Industrial potentials of saccharomyces cerevisiae. British Journal of Multidisciplinary and Advanced Studies 4(2):23–46

Parapouli M, Vasileiadis A, Afendra AS, et al (2020) Saccharomyces cerevisiae and its industrial applications. AIMS microbiology 6(1):1

Schuler MM, Sivaprakasam S, Freeland B, et al (2012) Investigation of the potential of biocalorimetry as a process analytical technology (pat) tool for monitoring and control of crabtree-negative yeast cultures. Applied microbiology and biotechnology 93:575–584

Sonnleitner B, Käppeli O (1986) Growth of saccharomyces cerevisiae is controlled by its limited respiratory capacity: formulation and verification of a hypothesis. Biotechnology and bioengineering 28(6):927–937

Sonntag D (1990) Important new values of the physical constants of 1986, vapor pressure formulations based on the its-90, and psychrometer formulae. Z Meteorol 70:340–344

Türker M (2004) Development of biocalorimetry as a technique for process monitoring and control in technical scale fermentations. Thermochimica Acta 419(1-2):73–81

Verduyn C, Zomerdijk TP, van Dijken JP, et al (1984) Continuous measurement of ethanol production by aerobic yeast suspensions with an enzyme electrode. Applied microbiology and biotechnology 19:181–185

Volesky B, Yerushalmi L, Luong J (1982) Metabolic-heat relation for aerobic yeast respiration and fermentation. Journal of Chemical Technology and Biotechnology 32(6):650–659

Von Stockar U, Maskow T, Liu J, et al (2006) Thermodynamics of microbial growth and metabolism: an analysis of the current situation. Journal of Biotechnology 121(4):517–533

Williams LA (1982) Heat release in alcoholic fermentation: a critical reappraisal. American Journal of Enology and Viticulture 33(3):149–153

Yang N, Guerin C, Kokanyan N, et al (2024) Raman spectroscopy applied to online monitoring of a bioreactor: Tackling the limit of detection. Spectrochimica Acta Part A: Molecular and Biomolecular Spectroscopy 304:123343